Fiber Bragg grating for spectral phase optical code-division multiple-access encoding and decoding

Xiaohui Fang

Department of Electrical Engineering, Hong Kong Polytechnic University, Hung Hom, Kowloon, Hong Kong, and College of Precision Instrument and Opto-Electronics Engineering, Tianjin University, Tianjin, China

Dong-Ning Wang

Department of Electrical Engineering, The Hong Kong Polytechnic University, Hung Hom, Kowloon, Hong Kong

Shichen Li

College of Precision Instrument and Opto-Electronics Engineering, Tianjin University, Tianjin, China

Received December 15, 2002; revised manuscript received April 1, 2003

A new method for realizing spectral phase optical code-division multiple-access (OCDMA) coding based on step chirped fiber Bragg gratings (SCFBGs) is proposed and the corresponding encoder/decoder is presented. With this method, a mapping code is introduced for the *m*-sequence address code and the phase shift can be inserted into the subgratings of the SCFBG according to the mapping code. The transfer matrix method together with Fourier transform is used to investigate the characteristics of the encoder/decoder. The factors that influence the correlation property of the encoder/decoder, including index modulation and bandwidth of the subgrating, are identified. The system structure is simple and good correlation output can be obtained. The performance of the OCDMA system based on SCFBGs has been analyzed. © 2003 Optical Society of America

OCIS codes: 060.1660, 060.2340.

1. INTRODUCTION

Optical code division multiple access (OCDMA) is a spread-spectrum technique that permits a large number of users to share the same bandwidth simultaneously but to be addressable individually through the allocation of specific address codes. With this technique, the encoded optical pulses are usually transmitted through a star network and received by the receiver designed to recognize the data bits with a specific address code. Such an address code recognition is usually achieved by matched filtering. In recent years, OCDMA as a multiplexing technique having great potential in high-speed local area networks has attracted much research interest because of its advantages such as flexible bandwidth usage, potentially good cross-talk performance, asynchronous access, and dynamic sharing of the channel resources.

The encoder/decoder is one of the key components in an OCDMA system that can be used either in the time domain or in the frequency domain. In the time domain, each data bit to be transmitted is represented by a code that consists of a series of pulses. The pulses contained in the coded bit are referred to as chips. While in the frequency domain, the total spectral band is divided into many small segments and the code information is contained in these segments.

For the optical fiber delay lines[1,2] that perform coding in the time domain or the fiber Bragg grating (FBG)-based encoder/decoder that operates either in the time domain[3] or in the frequency domain,[4,5] unipolar codes that exhibit poor correlation property and support only a small number of simultaneous users are widely used. For a traditional free-space grating-pair (FSGP) encoder/decoder[6,7] that operates in the frequency domain, bipolar codes can be employed through a phase-coding scheme. The use of phase coding is of great interest to OCDMA, since the bipolar codes adopted in the phase-coding scheme exhibit good correlation property, low interchannel interference, and support a relatively large number of simultaneous users for a given code length. However, a FSGP encoder/decoder suffers the drawback of poor coupling efficiency in optical fibers.

The OCDMA encoder/decoder based on fiber gratings possesses the advantages of easy device fabrication and compatibility with optical fiber communication systems. In recent years, the rapid development of FBG fabrication technology has reached a stage at which the optical phase of the light reflected from an individual grating can be accurately controlled, which allows the optical phase to be used as a coding parameter[8,9] and thus opens the way to use FBGs to perform effective encoding/decoding functions in an OCDMA system.[10–14]

A spectral phase encoder/decoder based on a step chirped fiber Bragg grating (SCFBG) has been experimentally demonstrated by Grunnet-Jepsen *et al.*[12–14] The SCFBG originates from traditional spectral phase encoding/decoding by use of a FSGP configuration[6,7] and

0740-3224/2003/081603-08$15.00

has the advantage of high-coupling efficiency in optical fibers. Additional theoretical analysis is still needed to improve the performance of this kind of OCDMA encoder/decoder. The coding scheme based on a SCFBG must be designed differently from that based on a FSGP in which the phase shift on each pixel on the spatial mask is independent from each other. However, in the encoder/decoder based on a SCFBG, the phase shift of one of the subgratings influences not only the phase of the reflection coefficients of its own subgrating but also all the subgratings connected subsequently, i.e., the phase shift on any subgrating is not independent of each other.

Here we propose a new method for realizing spectral phase coding based on SCFBGs and present the corresponding structure of an encoder/decoder. In this method, a mapping code is introduced to the address code and the corresponding phase shift is inserted into subgratings of a SGFBG according to the mapping code. The transfer matrix method together with the Fourier transform is used to investigate the transmission characteristics of the encoder/decoder. The factors that influence the correlation property of the system are identified.

2. STRUCTURE OF THE OPTICAL CODE DIVISION MULTIPLE ACCESS SPECTRAL ENCODER/DECODER BASED ON STEP CHIRPED FIBER BRAGG GRATINGS

Figure 1 is a schematic diagram of an encoder/decoder based on SCFBGs. Figure 1(a) is an encoder and Fig. 1(b) represents a decoder that matches the encoder in Fig. 1(a). The encoder consists of a pair of SCFBGs in a series arrangement. When an input bit (ultrashort pulse) is incident on the first SCFBG, G1, the wavelength components are dispersed and the reflected pulse is temporally expanded. When this expanded bit is reflected by the second SCFBG, G2, which exhibits opposite dispersion slope to G1, the wavelength components are resynchronized and the original pulse is reconstructed. However, in G2, if the phase shifts are incorporated into the subgratings according to their corresponding address code, the output pulse then represents a spectral phase-encoded bit. The encoded data bit subsequently transmits through the network before it reaches the receiver. The decoder consists of a pair of SCFBGs, G3 and G4, which are essentially the same as G1 and G2, but connected to the circulator in reverse order. The phase shifts are incorporated into the subgratings of G4 according to the same address code as that of the encoder but in reverse order when compared with that of G2. After the encoded data bit passed through the matched decoder, spectral phase shifts are compensated and the original coherent ultrashort pulse is reconstructed. On the other hand, if the decoder does not match the encoder, the spectral phase shifts are rearranged but not necessarily compensated, and the pulse at the output of the decoder is still a low intensity pseudonoise burst, which is known as multiple access interference. The threshold device is used to detect the data that corresponds to relatively high intensity and properly decoded pulses and to reject relatively low intensity and improperly decoded pseudonoise bursts.

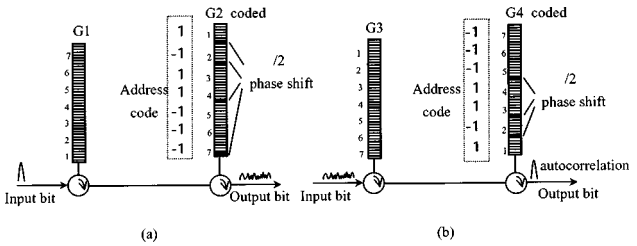

Fig. 1. Schematic diagram of an all-fiber encoder/decoder based on SCFBGs: (a) encoder and (b) matched decoder.

3. OPERATING PRINCIPLE OF ENCODING/DECODING BASED ON STEP CHIRPED FIBER BRAGG GRATINGS

A. Transmission Characteristics of Step Chirped Fiber Bragg Gratings with or without Phase Shift

For the SCFBG used in an encoder/decoder, the reflection spectral bandwidth for each subgrating should be the same. Considering the weak coupling condition $\kappa\Delta z \ll \pi^2$, the bandwidth between the spectral peak and the first zero position in the reflection spectrum of a uniform subgrating is given by Eq. (1):

$$\Delta\lambda = \frac{\lambda^2}{2n_{\text{eff}}\Delta z}, \tag{1}$$

where $\kappa = (\pi\Delta n/\lambda n_{\text{eff}})$ is the coupling index, Δn is the index modulation, λ is the wavelength in vacuum, n_{eff} is the effective mode index of a FBG, and Δz is the length of the subgrating.

The transfer matrix method is used to investigate the transmission characteristics of an encoder/decoder based on SCFBGs. For a SCFBG, its transfer matrix can be written as[15]

$$T(0, L) = \left[\prod_{n=N}^{2} T_n(z_{n-1}, z_n)\Phi_n\right] T_1(z_0, z_1), \tag{2}$$

where $z_0 = 0$, $z_N = L$, and $T_n(z_{n-1}, z_n)$ represents the transfer matrix of a subgrating:

$$T_n(z_{n-1}, z_n) = \begin{Bmatrix} \exp[-i\,\delta\beta_n(z_n - z_{n-1})]p_n & \exp[-i\,\delta\beta_n(z_n + z_{n-1})]q_n \\ \exp[i\,\delta\beta_n(z_n + z_{n-1})]q_n^* & \exp[i\,\delta\beta_n(z_n - z_{n-1})]p_n^* \end{Bmatrix}, \tag{3}$$

$$p_n(z_n - z_{n-1}) = \left\{\cosh[\alpha_n(z_n - z_{n-1})] + i\frac{\delta\beta_n}{\alpha_n}\sinh[\alpha_n(z_n - z_{n-1})]\right\}, \tag{4}$$

$$q_n(z_n - z_{n-1}) = i\frac{\kappa_n}{\alpha_n}\sinh[\alpha_n(z_n - z_{n-1})], \tag{5}$$

where p_n^* and q_n^* are the complex conjugates of p_n and q_n, respectively, $\delta\beta_n = 2\pi(\lambda^{-1} - \lambda_n^{-1})$ is the detuning from the Bragg wavelength of the nth subgrating λ_n, $\alpha_n = [|\kappa_n|^2 - (\delta\beta_n)^2]^{1/2}$, and Φ_n is the transfer matrix that corresponds to the phase shift of $\varphi_n/2$ inserted between the $(n-1)$th and nth step subgrating:

$$\Phi_n = \begin{bmatrix} \exp(i\varphi_n/2) & 0 \\ 0 & \exp(-i\varphi_n/2) \end{bmatrix}. \tag{6}$$

The reflection coefficient is[13]

$$r = -(T_{21}/T_{22}). \tag{7}$$

When Δn is small and there is only a slight overlap between the central peaks of the adjacent reflection spectrum, for spectral band $\lambda_n \pm \Delta\lambda$ (corresponding to the Bragg wavelength of the nth subgrating), $\delta\beta_n$ is small and even becomes zero when the phase of the forward wave and the phase of the backward wave match. Whereas $\delta\beta_m (m \in \{1, N\}, m \neq n)$ of the other subgrating is large. When Δn is small and $\delta\beta_m \gg \kappa$, then $\alpha_m = (\kappa^2 - \delta\beta_m^2)^{1/2} \approx i\delta\beta_m$, and we have $q_m \approx 0$. Thus according to Eqs. (2)–(5), the reflection characteristics within spectral band $\lambda_n \pm \Delta\lambda$ can be approximately expressed by the reflection coefficient of the nth subgrating:

$$r_n \approx -\frac{q_n^*}{p_n^*}\exp(i\delta\beta_n z_{n-1}). \tag{8}$$

When there are phase shifts between the subgratings,

$$r_n \approx -\frac{q_n^*}{p_n^*}\exp(i\delta\beta_n z_{n-1})\exp\left(i\sum_{l=1}^{n}\varphi_l\right), \tag{9}$$

where $\varphi_l/2$ is the phase shift between the $(l-1)$th and lth subgrating. Comparing approximation (8) with approximation (9), the phase shifts between subgratings produce a term of additional phase shift $\Sigma_{l=1}^{n}\varphi_l$ only, which is the two times sum of phase shifts inserted between subgratings before the nth subgrating, for reflection coefficient r_n. The total reflection coefficient is the sum of the reflection coefficients of all the subgratings:

$$r \approx \sum_{n=1}^{N} r_n. \tag{10}$$

B. Realization of Phase Coding in a Step Chirped Fiber Bragg Grating

The m sequence is used as the address code in our system. Assigning an address code to the kth and vth user, respectively, $c^k = (c_1^k, c_2^k, \ldots, c_N^k)$ and $c^v = (c_1^v, c_2^v, \ldots, c_N^v)$, where $c_n^{k,v} \in \{1, -1\}$ and $k, v \in \{1, N\}$. We consider the sequence c^v as being $(\rho^l c^k) = (c^k)^l$, where ρ is the operator that shifts vectors cyclically to the left by one place, that is, $(\rho c^k) = (c_2^k, c_3^k, \ldots, c_{N-1}^k, c_1^k)$, in which case the correlation function of c^k and c^v can be written as

$$\theta_{kv}(l) = \frac{1}{N}\sum_{i=1}^{N} c_i^k c_i^v = \frac{1}{N}\sum_{i=1}^{N} c_i^k c_{i+l}^k, \tag{11}$$

which results in $\theta_{kv}(0) = 1$ for $l = 0$ and $\theta_{kv}(l) = 1/N$ for $l = 1$ to N. By assigning N cycle shifts to N subscribers, one can obtain an OCDMA network that supports up to N simultaneous users. In Eq. (9), if $\varphi_l^k/2 \in \{\pi/2, 0\}$ and $\exp(i\Sigma_{l=1}^{n}\varphi_l^k) = c_n^k$, the SCFBG with incorporated phase shifts represents an OCDMA encoder/decoder. To satisfy the condition $\exp(i\Sigma_{l=1}^{n}\varphi_l^k) = c_n^k$, an address code mapping needs to be established: no change for the first code element; for the others, each must be compared with the previous code element. If they are the same, the mapping code element is 1, otherwise -1. Thus a mapping code is established. For example, the mapping code of the m-sequence address code with a length of 7, $(-1, -1, -1, 1, 1, -1, 1)$, is $(-1, 1, 1, -1, 1, -1, -1)$. The sequence elements $\varphi_l^k/2 \in \{\pi/2, 0\}$, $l \in \{1, N\}$, corresponding to $\{-1, 1\}$ of the mapping code element, is added in front of the corresponding subgrating. Thus, for G2 in Fig. 1, from $\lambda_7 \pm \Delta\lambda$ to $\lambda_1 \pm \Delta\lambda$, the additional phase shifts of the reflection coefficient for the subgratings in G2 are $\{\phi_n^k\} = \{\Sigma_{l=1}^{n}\varphi_l^k\} = \{\pi, \pi, \pi, 2\pi, 2\pi, 3\pi, 4\pi\}$, corresponding to the address code $(-1, -1, -1, 1, 1, -1, 1)$.

An ideal spectral OCDMA encoding/decoding scheme based on SCFBGs should satisfy the condition that the spectral band of each subgrating has a flat top and there is neither overlap nor gap between adjacent spectral bands. Thus according to approximations (8) and (9), the reflection coefficients of the spectral band $\lambda_n \pm \Delta\lambda$ for G1 and G2, respectively, can simply be written as

$$r_n \approx i\tanh[\kappa(z_n - z_{n-1})]\exp(i\delta\beta_n z_{n-1}), \quad \lambda \in \lambda_n \pm \Delta\lambda, \tag{12}$$

$$r_n \approx i\tanh[\kappa(z_n - z_{n-1})]\exp[i\delta\beta_{(N+1-n)} z_{n-1}] \times \exp\left(i\sum_{l=1}^{n}\varphi_l^k\right), \quad \lambda \in \lambda_n \pm \Delta\lambda. \tag{13}$$

If the power spectrum of the input pulse is a constant over the entire spectral bandwidth, with an inverse Fourier transform, the time domain expression of the field amplitude for the optical pulse that passes through G1 and G2 in the encoder can be written, respectively, as

$$C_{1k}(t) \approx i\tanh(\kappa\Delta z)\frac{\sqrt{P_0}}{N}\sum_{n=1}^{N}\sin c[\pi\Delta f(t + 2t_{n-1})] \times \exp(i2\pi f_n t), \tag{14}$$

$$C_{2k}(t) \approx -\frac{\sqrt{P_0}}{N}\tanh^2(\kappa\Delta z)\sin c[\pi\Delta f(t + 2t_{N-1})] \times \sum_{n=1}^{N}\exp(i2\pi n f_n t)\exp\left(i\sum_{l=1}^{n}\varphi_l^k\right) = -\frac{\sqrt{P_0}}{N}\tanh^2(\kappa\Delta z)\sin c[\pi\Delta f(t + 2t_{N-1})] \times \sum_{n=1}^{N} c_n^k \exp(i2\pi f_n t), \tag{15}$$

where P_0 is the total power of the input pulse, $f_n = c/\lambda_n$, $\Delta f = c\Delta\lambda/\lambda_0^2$ (λ_0 is the central wavelength of the SCFBG), and $t_{n-1} = (n_{\text{eff}} z_{n-1})/c$ is the time delay associated with each spectral band, which represents the dispersion property of the chirped fiber grating. After the signal pulse passes through G2, which exhibits an op-

posite dispersion slope to G1, the dispersion obtained from G1 can be compensated by G2. In other words, the same time delay $2t_{N-1}$ can be obtained for all the spectral segments. Thus if no phase shift exists between any pair of subgratings of G2, the pulse will be reconstructed; otherwise, the pulse represents a spectral phase-encoded bit.

Since the phase shifts are incorporated into subgratings of the SCFBG in the encoder according to the mapping code, and as we have in Subsection 3.B, the bigger additional phase shift will be obtained for the reflection efficiency of the latter subgrating before which the pulse experiences more subgratings. To compensate the additional phase shift in the reflection coefficient, the step dispersion order of G4 in the decoder is set to be opposite that of G2 in the encoder. Hence, the code elements in the decoder are also set to be in reverse order with those in the encoder as shown in Fig. 1(b). Thus from $\lambda_1 \pm \Delta\lambda$ to $\lambda_7 \pm \Delta\lambda$, the additional phase shifts of the reflection coefficient for subgratings in G4 are $\{\phi_n^k\} = \{\Sigma_{l=1}^n \varphi_l^k\} = \{0, \pi, 2\pi, 2\pi, 3\pi, 3\pi, 3\pi\}$. If the decoder does not match the encoder, no compensation can be provided, and a cross-correlation output will appear. The electric field representation of the kth decoder output can be written as

$$E_k(t) = C_{kk}(t) + \sum_{k \neq v} C_{vk}(t - t'_{vk}), \tag{16}$$

where $C_{kk}(t)$ is the autocorrelation term, $\Sigma_{k \neq v} C_{vk}(t - t'_{vk})$ is the cross-correlation term that is a multiple access interference term, and t_{vk} denotes the random time delay between the arrival of the kth and the vth encoded signals at decoder k. If $t'_{kk} = 0$ is assumed, then perfect synchronization can be maintained between the desired transmitter and the receiver pair.

It should be noted that, if the first code element of the mapping code is -1, no phase shift is required to be added to the first subgrating; and the whole reflection spectral band will undergo an additional phase shift of $-\pi$, which actually has no effect on the final correlation output.

C. Correlation Property of the Encoder/Decoder Based on Step Chirped Fiber Bragg Gratings

A numerical simulation method is used to investigate the feasibility and performance of the proposed system. The correlation property of encoder/decoder based on SCFBGs is simulated by use of the transfer matrix method[10] and a Fourier transform. A series of Gaussian-shaped pulse trains of 0.1-ps pulse width is introduced to the encoder. The configuration of encoder/decoder is shown in Fig. 1, where an m-sequence address code with a code length of 7 is demonstrated for simplicity. Actually the m sequence with a code length of 15 is used as the address code, thus SCFBG consists of 15 subgratings, each of 2.7-mm length, and a bandwidth of approximately 0.3 nm. Bragg wavelengths of subgratings are increased in steps of 0.3 nm from 1540.3 to 1545.0 nm. The effective mode index $n_{\text{eff}} = 1.456$ and $\Delta n = 2.5 \times 10^{-4}$ are used in the simulations.

Figure 2 shows the reflection spectrum of G1, from which the reflection spectrum of an individual subgrating cannot be observed because of the overlap between neighboring spectral bands. In contrast, the sidelobe structure of the reflection spectrum of an individual subgrating has only a slight influence on the total reflection spectrum.

Figure 3 displays the dispersion of the pulse at the output of G1 in the encoder. It can be seen from this figure that there are 15 peaks that correspond to the time delay of 15 subgratings. The value of the step time delay is given approximately by $t_{n-1} = (n_{\text{eff}} z_{n-1})/c$ in approximation (14), which is a simplified expression of the transmission characteristics of the encoder/decoder. It should also be noted that the intensity of the first subpulse is much higher than that of the others, as the intensity of each subpulse except the first is reduced because of the reflection spectrum overlap between adjacent subgratings. In addition, subgrating sidelobes cause the dispersed subpulse distortion. When Δn is increased, the side-mode structure increases rapidly, resulting in greater distortion.

The correlation output curve of the decoder obtained with the m sequence as the address code with a code length of 15 is demonstrated in Fig. 4. When the decoder matches the encoder, there is an autocorrelation output as shown in Fig. 4(a); otherwise, cross-correlation output appears as shown in Fig. 4(b), where the address code (1, 1, -1, 1, 1, -1, -1, 1, -1, 1, -1, -1, -1, -1, 1) is added to G4.

A number of factors such as index modulation Δn and the bandwidth of the subgrating can influence the correlation property of an encoder/decoder based on a SCFBG. To satisfy Eq. (8) and approximation (9), a small Δn is required for an encoder/decoder based on SCFBGs. Figure 5 demonstrates the autocorrelation and cross-correlation output curves that correspond to different values of Δn. When $\Delta n = 1 \times 10^{-3}$, it is difficult to distinguish the autocorrelation and the cross-correlation outputs as shown in Fig. 5(a). If $\Delta n = 3.5 \times 10^{-4}$, the intensity ratio of

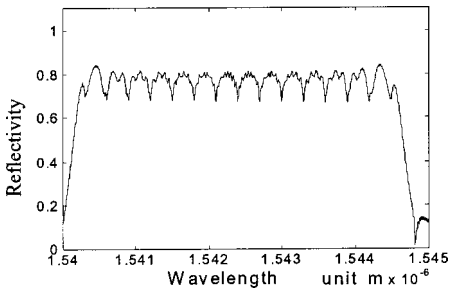

Fig. 2. Reflection spectrum of SCFBG G1.

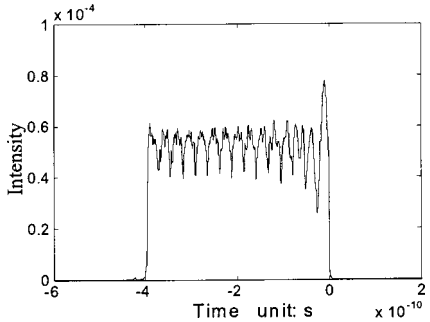

Fig. 3. Pulse dispersion at the output of G1.

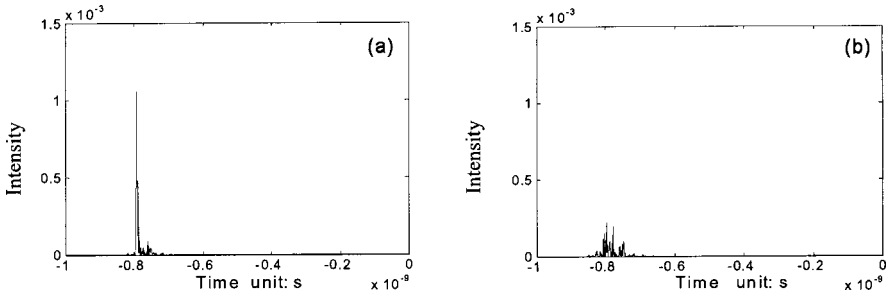

Fig. 4. Correlation curve based on a SCFBG decoder with an m-sequence code of code length 15: (a) autocorrelation curve for the signal that passes through the matched decoder and (b) cross-correlation curve for the signal that passes through the mismatched decoder.

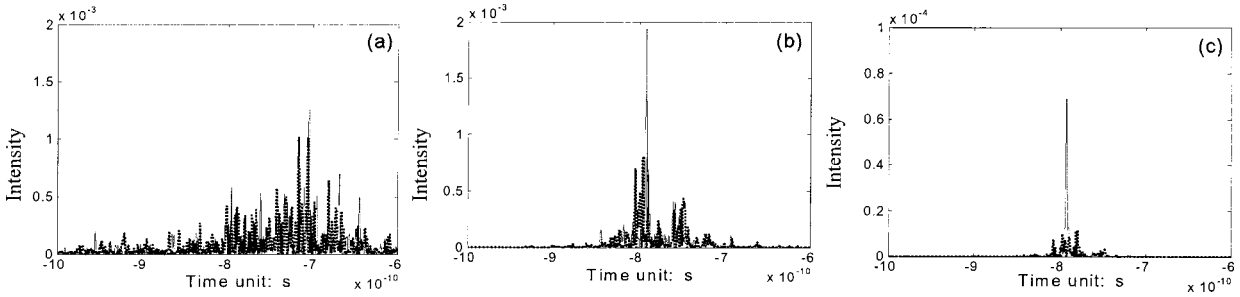

Fig. 5. Correlation curves correspond to different Δn. The solid lines represent the autocorrelation curves and the dotted lines represent the cross-correlation curves: (a) $\Delta n = 1 \times 10^{-3}$, (b) $\Delta n = 3.5 \times 10^{-4}$, (c) $\Delta n = 1.5 \times 10^{-4}$.

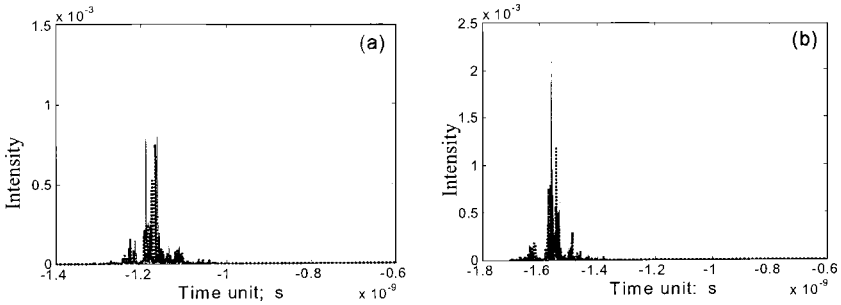

Fig. 6. Correlation curves correspond to different reflection bandwidths of subgratings. The solid lines represent the autocorrelation curve and the dotted lines represent the cross-correlation curves: (a) $\Delta\lambda = 0.2$ nm and (b) $\Delta\lambda = 0.15$ nm.

the autocorrelation to the cross correlation becomes 2.4:1, and the autocorrelation output can be clearly recognized as demonstrated in Fig. 5(b). For $\Delta n = 1.5 \times 10^{-4}$, the intensity ratio reaches 7:1 and the autocorrelation output becomes extremely dominant as shown in Fig. 5(c).

Another important parameter that determines the correlation output of the system is the reflection spectrum bandwidth. In Eq. (16), the autocorrelation term $C_{kk}(t)$ is similar to $C_{2k}(t)$ and can be expressed as

$$C_{kk} = -\frac{\sqrt{P_0}}{N}\tanh^4(\kappa\Delta z)\sin c[\pi\Delta f(t + 4t_{N-1})] \times \sum_{n=1}^{N}\exp(i2\pi f_n t),$$

$$C_{kk}C_{kk}^{*} = -\frac{P_0}{N^2}\tanh^8(\kappa\Delta z)\sin c^2[\pi\Delta f(t + 4t_{N-1})] \times \left[\sum_{n=1}^{N}\exp(i2\pi f_n t)\right]\mathrm{cc} = -\frac{P_0}{N^2}\tanh^8(\kappa\Delta z)\sin c^2[\pi\Delta f(t + 4t_{N-1})] \times \frac{\sin^2(\pi N\Delta f t)}{\sin^2(\pi\Delta f t)}. \quad (17)$$

The term $[\sin^2(\pi N\Delta f t)]/[\sin^2(\pi\Delta f t)]$ has a comblike structure with period $T_N = (1/N\Delta f)$. Only when time delay $4t_{N-1}$ in approximation (17) is a multiple of T_N is there an overlap between one of the peaks in the comblike

structure and the peak of $\sin c[\pi\Delta f(t + 4t_{N-1})]$. As a result, the maximum autocorrelation peak can be obtained; otherwise the autocorrelation peak could decrease sharply. According to Eq. (1), under the condition that the bandwidth $\Delta\lambda$ in the reflection spectrum of the subgrating is equal to the Bragg wavelength increase/decrease of the adjacent subgratings, i.e., $\delta\lambda = \lambda_{B_n}\lambda_{B_{n-1}}$, where λ_{B_n} is the Bragg wavelength of the nth subgrating, we have $4t_{N-1}/T_N = 2N(N-1)$ and the maximum autocorrelation will appear. While $\Delta\lambda$=0.2 nm and $\delta\lambda$=0.3 nm, the time delay $4t_{N-1}$ is not a multiple of T_N, and thus the correlation property is poor as shown in Fig. 6(a). In Fig. 6(b), $\Delta\lambda = 0.15$ nm, and $\delta\lambda$ is still 0.3 nm, the time delay $4t_{N-1}$ is a multiple of T_N, and the spectral bandwidth of each subgrating is half of that in Figs. 4 and 5. Thus the length of each subgrating and hence the time delay is double that in Figs. 4 and 5, and the peak of the comblike structure at the $4t_{N-1}$ position decreases sharply. As a result, the correlation property becomes worse than that in Figs. 4 and 5. To obtain a good correlation property, a large code length is required, but a proper selection of other parameters such as Δn and the bandwidth is also essential. From Fig. 6 it can be seen that good correlation property can be obtained only when the bandwidth of the reflection spectrum of each subgrating is equal to the difference between Bragg wavelengths of the neighboring subgratings, i.e., $\Delta\lambda = \delta\lambda$. There are two ways to increase the code length. The first is to increase the number of subgratings without any change of $\Delta\lambda$, which thus increases the total bandwidth. The second is to use a narrow bandwidth $\Delta\lambda$ without any change in total bandwidth. However, the relation $\Delta\lambda = \delta\lambda$ also needs to be satisfied in this case.

4. PERFORMANCE ANALYSIS

Figure 7 shows block diagrams of a coherent ultrashort light pulse OCDMA transmitter and receiver. In Fig. 7(a), the data source is first encoded by an on–off keying (OOK) encoder. The pulses generated are sent to an OCDMA encoder based on SCFBGs, an m-sequence address code is assigned to each data pulse, and the output pulses represent the spectral phase of OCDMA encoded signals. Figure 7(b) represents a receiver for an ultrashort pulse OCDMA communication system. The kth receiver is assumed to be a correlation receiver matched to the kth transmitter.

In our system, the shot noise and the thermal noise of the receiver are neglected because multiple access interference is the main noise factor, and it is assumed that

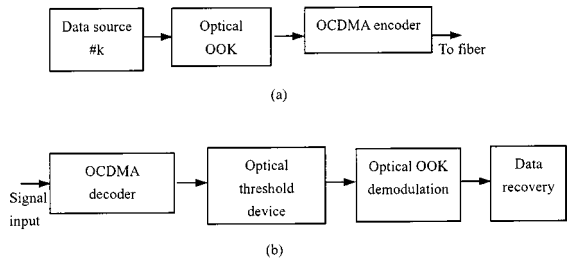

Fig. 7. Coherent ultrashort light pulse OCDMA (a) transmitter and (b) receiver pair.

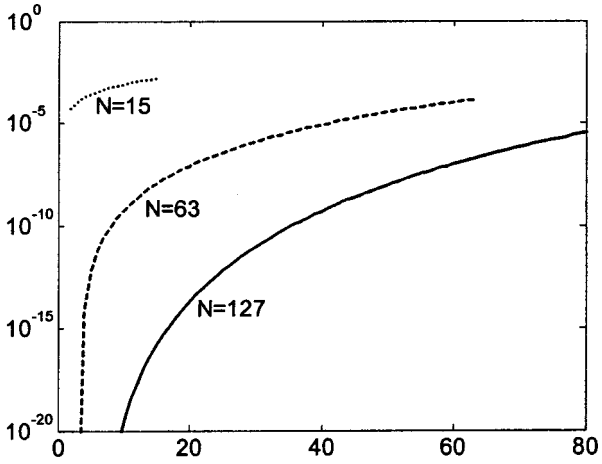

Fig. 8. BER versus the number of simultaneous users.

communication between each transmitter and receiver pair is continuous. Pseudonoise bursts generated by spectral phase coding based on SCFBGs are not stationary random processes in a strict sense, hence it is also difficult to calculate the bit error rate (BER) of the system precisely. However, when Δn in SCFBGs is small and there are a large number of simultaneous users with long m sequences as the address codes in the decoder,[16,17] the unsuccessfully decoded pulse can be assumed to be a Gaussian random process.

For a single user case the intensity signal I has a chi-square probability density function and can be shown to be

$$p(x) = \frac{1}{\sigma^2}\exp(-x/\sigma^2), \tag{18}$$

where variance $\sigma = 1.263\sqrt{T_0/T_\sigma}$, T_0 is the initial pulse width, the root-mean-square width of encoded pulse $T_\sigma \approx T_0 N/\sqrt{2}$, and N is the code length. Although multiple undesired users interfere with the desired user, the total interference can be taken as the summation of independent multiple random processes whose probability density function is

$$p_n(x) = \frac{x^{n-1}}{\sigma^{2n}(n-1)!}\exp(-x/\sigma^2). \tag{19}$$

When the number of undesired users is large, according to the central limit theorem

$$p_n(x) \approx N(n\sigma^2, n\sigma^4). \tag{20}$$

In the following we denote the photocurrent detected by the photodetector of the kth receiver as the random variable Y^k, and I_{th} as the threshold of the decoder. Then the BER of such a system can be expressed as

$$\text{BER} = \frac{1}{2}[Pr(Y^k > I_{\text{th}}|b_n^k = 0) + Pr(Y^k \leqslant I_{\text{th}}|b_i^k = 1)], \tag{21}$$

where[17]

$$Pr(Y^k > I_{\text{th}} | b_i^k = 0) = \sum_{i=1}^{n-1} \binom{n-1}{i} p^i (1-p)^{n-1-i} \times \int_{I_{\text{th}}}^{\infty} \frac{1}{\sqrt{2\pi n}\sigma^2} \exp\left[-\frac{(x - i\sigma^2)^2}{2i\sigma^4} \right] dx, \quad (22)$$

$$Pr(Y^k \leqslant I_{\text{th}} | b_i^k = 1)] = \sum_{i=1}^{n-1} \binom{n-1}{i} p^i (1-p)^{n-1-i} \times \int_{-\infty}^{I_{\text{th}}} \frac{1}{\sqrt{2\pi n}\sigma^2} \exp\left[-\frac{(x - i\sigma^2 - 1)^2}{2i\sigma^4} \right] dx, \quad (23)$$

where $p = (1/2)(T_\sigma/T_b)$ and T_b is the period of the data source.

Figure 8 depicts the BER versus the number of simultaneous users when the code length is 15, 63, and 127, respectively. $T_0 = 0.1$ ps and $T_b = 50$ ps for all the users. From Fig. 8 it is obvious that the longer the code length, the more simultaneous users the system can support.

5. FABRICATION OF SPECIALLY DESIGNED STEP CHIRPED FIBER BRAGG GRATINGS

With the development of fabrication technology for fiber gratings, it is possible to fabricate SCFBGs with precise control of the phase shift that needs to be incorporated into the subgrating. The most direct method is to use the phase mask with a specially designed phase shift, but such a method is expensive. Another method is the so-called continuous grating writing technique,[11,18] which effectively writes gratings on a grating plane and allows for fabrication of gratings with truly complex refractive-index profiles. This technique uses a simple phase mask with a uniform pitch and relies on precise control of the positioning of the fiber relative to the mask and the exposure of ultraviolet light used to write the grating. A single phase mask can thus be used to write a wide range of complex grating structures.

6. SUMMARY

We have proposed a new method for realizing spectral phase OCDMA coding based on SCFBGs and presented the corresponding structure of an encoder/decoder. With this method, a mapping code has been introduced and the designed phase shift was inserted into the corresponding subgrating of a SCFBG according to the mapping code. The factors that influence the correlation property of an encoder/decoder include index modulation Δn and the bandwidth of the subgrating. The structure of an encoder/decoder is simple and good correlation property can be readily obtained. The system performance analysis shows that, when Δn is small and the code length of the m sequence is long enough, the unsuccessfully decoded pulse can be treated as a Gaussian random process.

ACKNOWLEDGMENT

This research is partially supported by Hong Kong Polytechnic University Research grant G-YC89.

X. Fang's e-mail address is eexhfang@polyu.edu.hk.

REFERENCES

1. M. E. Marhic, "Coherent optical CDMA networks," J. Lightwave Technol. **11**, 854–863 (1993).
2. J. G. Zhang and G. Picchi, "Tunable prime-code encoder/decoder for all-optical CDMA applications," Electron. Lett. **29**, 1211–1212 (1993).
3. P. C. Teh, J. H. Lee, M. Ibsen, P. Petropoulos, and D. J. Richardson, "A 10-Gbit/s all-optical code generation and recognition system based on a hybrid approach of optical fiber delay line and superstructure fiber Bragg grating technologies," in *Optical Fiber Communication Conference*, Vol. 54 of OSA Trends in Optics and Photonics (Optical Society of America, Washington, D.C., 2001), pp. WDD91-WD1-3.
4. L. R. Chen and P. W. E. Smith, "Demonstration of incoherent wavelength-encoding/time-spreading optical CDMA using chirped moire gratings," IEEE Photonics Technol. Lett. **12**, 1281–1283 (2000).
5. Z. Wei, H. Ghafoui-Shiraz, and H. M. H. Shalaby, "New code families for fiber-Bragg-grating-based spectral amplitude-coding optical CDMA systems," IEEE Photonics Technol. Lett. **13**, 890–892 (2001).
6. M. M. Wefers and K. A. Nelson, "Programmable phase and amplitude femtosecond pulse shaping," Opt. Lett. **18**, 2032–2034 (1993).
7. K. Kamakura, T. Ohtsuki, and I. Sasase, "Optical spread time CDMA communication systems with PPM signaling," IEICE Trans. Fundam. Electron. Commun. Comut. Sci. **E82-B**, 1038–1047 (1999).
8. Y. Nasu and S. Yamashita, "Multiple phase-shift superstructure fibre Bragg grating for DWDM systems," Electron. Lett. **37**, 1471–1472 (2001).
9. P. Petropoulos, M. Ibsen, A. D. Ellis, and D. J. Richardson, "Rectangular pulse generation based on pulse reshaping using a superstructured fiber Bragg grating," J. Lightwave Technol. **19**, 746–752 (2001).
10. P. C. Teh, P. Petropoulos, M. Ibsen, and D. J. Richardson, "Phase encoding and decoding of short pulses at 10 Gb/s using superstructured fiber Bragg gratings," IEEE Photon. Technol. Lett. **13**, 154–156 (2001).
11. P. C. Teh, M. Ibsen, J. H. Lee, P. Petropoulos, and D. J. Richardson, "A 4-channel WDM/OCDMA system incorporating 255-chip, 320 Gchip/s quaternary phase coding and decoding gratings," in *Optical Fiber Communication Conference*, Vol. 54 of OSA Trends in Optics and Photonics (Optical Society of America, Washington, D.C., 2001), PD37-1-PD37-3.
12. A. Grunnet-Jepsen, A. E. Johnson, E. S. Maniloff, T. W. Mossberg, M. J. Munroe, and J. N. Sweetser, "Fibre Bragg grating based spectral encoder/decoder for lightwave CDMA," Electron. Lett. **35**, 1096–1097 (1999).
13. A. Grunnet-Jepsen, A. E. Johnson, E. S. Maniloff, T. W. Mossberg, M. J. Munroe, and J. N. Sweetser, "Demonstration of all-fiber sparse lightwave CDMA based on temporal phase encoding," IEEE Photon. Technol. Lett. **11**, 1283–1285 (1999).
14. J. N. Sweetser, A. E. Johnson, and A. Grunnet-Jepsen, "Demonstration of code-division multiplexing with synchronous orthogonal coding using fiber Bragg gratings," in *Optical Fiber Communication Conference*, Vol. 54 of OSA Trends in Optics and Photonics (Optical Society of America, Washington, D.C., 2001), pp. ThH3-T1-3.

15. M. McCall, "On the application of coupled mode theory for modeling fiber Bragg gratings," J. Lightwave Technol. **18**, 236–242 (2000).
16. J. A. Salehi, A. M. Weiner, and J. P. Heritage, "Coherent ultrashort pulse code-division multiple access communication systems," J. Lightwave Technol. **8**, 478–491 (1990).
17. W. Ma, C. Zhou, H. Pu, and J. Lin, "Performance analysis of phase-encoded OCDMA communication system," J. Lightwave Technol. **20**, 770–775 (2002).
18. P. C. Teh, P. Petropoulos, M. Ibsen, and D. J. Richardson, "A comparative study of the performance of seven- and 63-chip optical code-division multiple-access encoders and decoders based on superstructured fiber Bragg gratings," J. Lightwave Technol. **19**, 1352–1365 (2001).